Opto-mechanical force measurement of deep sub-wavelength plasmonic modes

Kohoutek, John, Dey, Dibyendu, Bonakdar, Alireza, Sklar, Alejandro, Memis, Omer, et al.

John Kohoutek, Dibyendu Dey, Alireza Bonakdar, Alejandro Sklar, Omer Gokalp Memis, Ryan Gelfand, Hooman Mohseni, "Opto-mechanical force measurement of deep sub-wavelength plasmonic modes," Proc. SPIE 8097, Optical Trapping and Optical Micromanipulation VIII, 80971T (9 September 2011); doi: 10.1117/12.891888

Event: SPIE NanoScience + Engineering, 2011, San Diego, California, United States

Opto-mechanical force measurement of deep sub-wavelength plasmonic modes

John Kohoutek, Dibyendu Dey, Alireza Bonakdar, Alejandro Sklar, Omer Gokalp Memis, Ryan Gelfand, Hooman Mohseni

Bio-Inspired Sensors and Optoelectronics Laboratory (BISOL), EECS, Northwestern University, 2145 Sheridan Rd., Evanston, Illinois, USA

ABSTRACT

Spatial mapping of optical force near the hot-spot of a metal-dielectric-metal bow-tie nanoantenna at a wavelength of 1550 nm is presented. Non contact mode atomic force microscopy is used with a lock-in method to produce the map. Maxwell's stress tensor method has also been used to simulate the force produced by the bow-tie and it agrees with the experimental data. If dual lock-in amplifiers are used, this method could potentially produce the near field intensity and optical force map simultaneously, both with high spatial resolution. Detailed mapping of the optical force is critical for many emerging applications such as plasmonic biosensing and optomechanical switching.

1. INTRODUCTION

Photons have a momentum ($\hbar/\lambda$) and transfer of this momentum to other objects due to elastic scattering is the physical origin of radiation pressure and optical force. This has been known to exist since deduced by Maxwell in 1871 and has garnered much attention in the area of optical trapping when used in the far field [1-3]. Recently there has been even more interest to exploit the near-field region to generate an optical force to similarly trap particles [4-6]. Near-field trapping was demonstrated by Righini et. al in 2007 [7] and more recently has been used to trap even smaller particles [8]. However, so far little work has been done to map the near-field optical force at high resolution. If a large probe particle is used, the force of an optical trap has been mapped in the far field in 2006 [9] and the near field in the same year [10]. Optical force is generally related to Casimir force – whereas Casimir force is calculated using vacuum modes or "virtual" modes, optical force is calculated using actual modes, but both may be calculated using Maxwell's stress tensor formalism [6, 11]. Thus, it is on the heels of our work in measuring the Casimir force with high resolution [12] that we present a method to accurately map the optical force at high resolution [13].

2. SURFACE PLASMONS

A surface plasmon (SP) is a collective motion of electrons generated by light at the interface between two mediums of opposite sign of dielectric susceptibility (e.g. metal and dielectric)[14]. Optical antennas have previously been explored in the visible region[15] to exploit surface plasmon resonance (SPR). Optical antennas are similar to radio frequency (RF) antennas in that they are resonant structures that respond to specific wavelengths through the geometrical and material characteristics of the antenna as well as the surrounding environment. Though both RF and optical antennas have the same fundamental goal of controlling radiation patterns, there exists an underlying discrepancy. While RF antennas focus on optimization of far-field characteristics in order to obtain better transmission and reception performance, optical antennas emphasize the near field behavior to for example create a spot size that is smaller than the wavelength of incoming light.

Because the optical force originates from the divergence of the electromagnetic energy density [16], the fact that plasmonics can be used to concentrate the electric field to a very small spot can lead to a very large force density. Based on our simulation and experimental analysis [17, 18], we have chosen a metal-dielectric-metal

Optical Trapping and Optical Micromanipulation VIII, edited by Kishan Dholakia, Gabriel C. Spalding,
Proc. of SPIE Vol. 8097, 80971T · © 2011 SPIE · CCC code: 0277-786X/11/$18 · doi: 10.1117/12.891888

(MDM Au/SiO2/Au) bow-tie antenna design, due to its capability to generate higher near-field enhancement. To optimize the performance of our design, we simulated the structure using three-dimensional finite-difference time-domain (FDTD) method. The antenna consists of two triangular arms separated by a gap of nearly 50 nm. The bowtie is placed on the facet of a cleaved optical fiber. A plane wave is launched with polarization along the long axis of the bowtie with wavelength of 1550 nm as the source for all simulations. We used a thickness of 40 nm and 30 nm for Au and SiO2 respectively. To get the resonant length of the bow-tie, we found the average intensity enhancement in the gap between the arms at the level of the top metal surface as we varied the length of the arms of the bow-tie (see Figure 1). Very fine mesh size was used in the antenna region and PML boundary conditions were used at the simulation edge, which was placed very far away from the antenna region. Based on this simulation, a resonance length of 350 nm for one arm was chosen for the rest of simulation and fabrication.

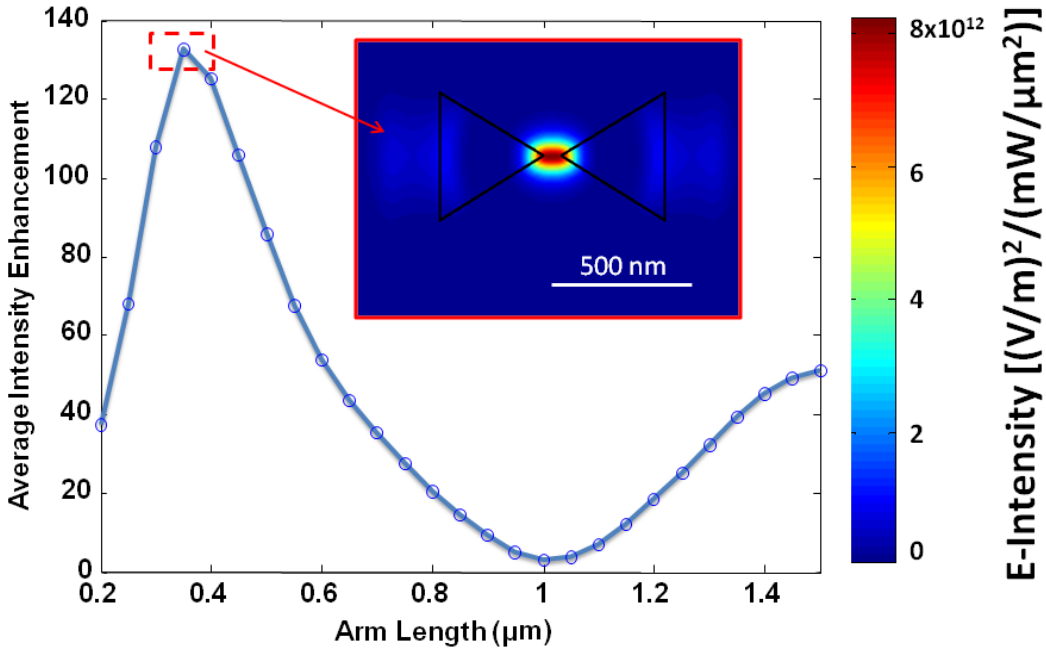

Figure 1 – Average intensity enhancement at the top surface of the antenna gap as a function of the bowtie arm length. (Inset) E-field intensity over the antenna region at the resonance condition. There is a central "hot-spot" and some signal at the edges of the arms as well.

After optimizing our design through simulation, we fabricated our design on the end of a cleaved 125 μm optical fiber. First, we coated the fiber with the correct MDM (Au/SiO2/Au) thicknesses described above via electron beam evaporation. The bow-tie structure was then fabricated using focused ion beam (FIB) milling (Hellios FEI). Using the gallium beam at high voltage (30 keV) and very low current (9.2 pA) a high precision milling was achieved. The final antenna along with the fiber face is shown in Figure 2.

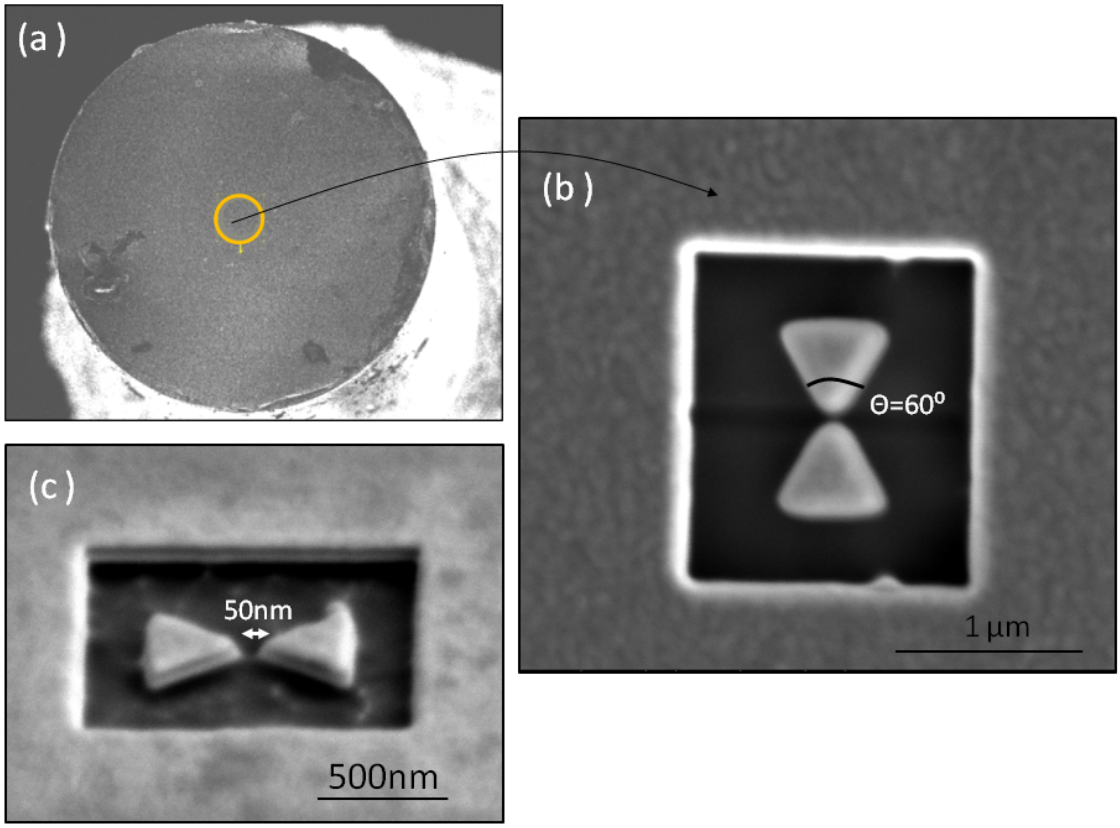

Figure 2 – (a) Coated face of cleaved optical fiber. The fiber is coated with 40nm/30nm/40nm Au/SiO2/Au. (b) Top-down view of bow-tie structure and surrounding box. (c) Oblique angle, showing sidewall angle.

We have then used apertureless near-field scanning optical microscopy (a-NSOM) to measure the near-field signal generated by our device. Our a-NSOM setup is a modification of a backscattered a-NSOM setup that we have previously used to characterize the near field of nanoantenna-integrated quantum cascade lasers [17-19]. A-NSOM was originally pioneered by Hillenbrand [20] to characterize near-field plasmonics. It works by light scattering off of a vibrating AFM tip and being modulated at that vibrational frequency. It then gets picked up by a detector which feeds into a lock-in amplifier, and the tip frequency is used as the reference. The output of the lock-in is fed to a computer which maps to the position of the AFM tip. The lock-in demodulates the signal and the output gives a map of the light which is scattered from the AFM tip with arbitrary gain. A figure depicting the setup we have used to characterize the near-field of our antennae is shown in Figure 3. The results of the near-field scan are shown in Figure 5e.

3. OPTICAL FORCE SIMULATION

We have used Maxwell's stress tensor method to calculate the optical force intensity on the AFM tip. Our simulation area consists of MDM box on top of an SiO2 layer which represents the fiber material. The bowtie is positioned in the center of the box with the correct sidewall angle created during fabrication. The AFM tip has been modeled as a sphere with diameter 100 nm (similar to actual diameter of AFM tip). The position of the sphere was varied, keeping the vertical height constant at 50 nm, and the electric field components at each position were recorded. As before, a single wavelength source was used and the polarization was kept along the long axis of the

bowtie. Six plane monitors were placed surrounding the sphere to get the electric and magnetic field components inside the monitor. The field components then are related to Maxwell's stress tensor by the following formula:

$$T_{ij} = \varepsilon_0 \varepsilon_m E_i E_j + \mu_0 \mu_m H_i H_j - \frac{1}{2}.\delta_{ij}(\varepsilon_0 \varepsilon_m \mid E \mid^2 + \mu_0 \mu_m \mid H \mid^2)$$

Where, E_i and H_i correspond to the electric and magnetic field, ε_m represents the electric permittivity, and μ_m represents the magnetic permeability for the object on which optical force is applied (AFM tip in our case). The force acting on the AFM tip has been calculated by the following formula:

$$< F_i >= \frac{1}{2}\mathrm{Re}\left(\int_S T_{ij}.n_j dS\right)$$

Where, n_j is the outward normal to the surface of the six planes mentioned before. Because the z-component of the optical force is calculated to be ~10 times larger than the in-plane (x and y) components, and this component would also have the largest effect on the amplitude of the AFM tip, we have only plotted this component. The final map can be seen in Figure 5d. It is important to note that although the force is attractive, creating a trap, we have only shown the magnitude of this force.

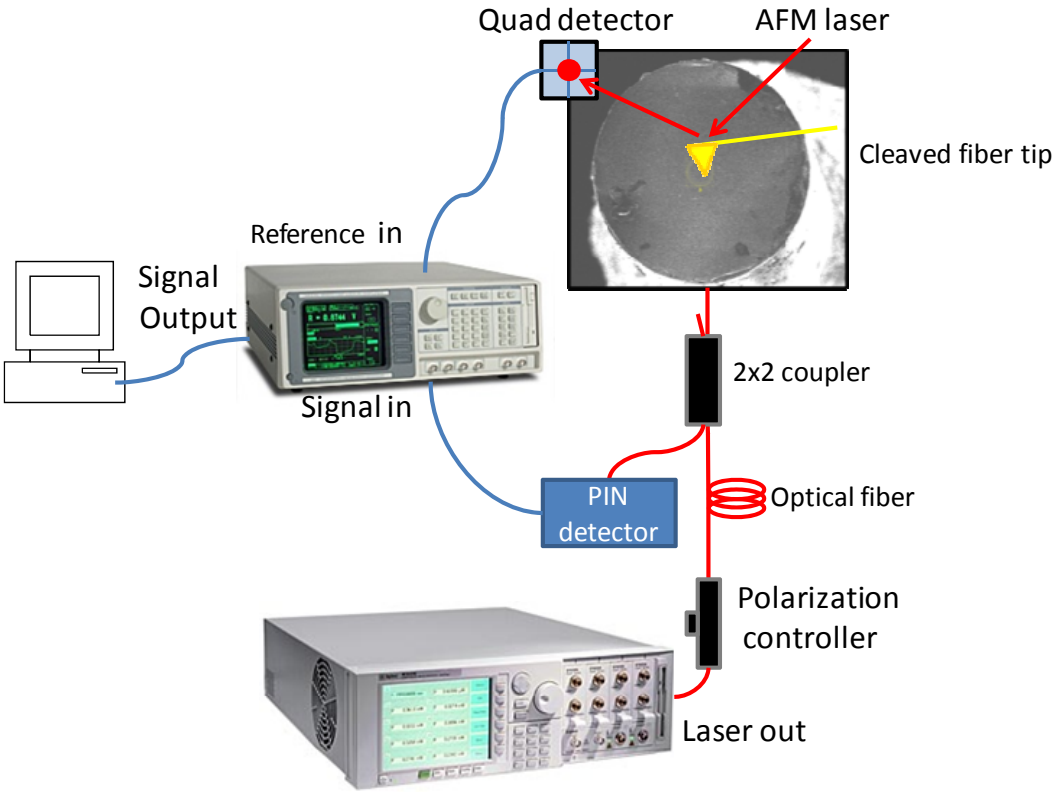

Figure 3 – Apertureless-NSOM setup used to visualize the near field of our bow-tie structures.

4. OPTICAL FORCE MEASUREMENT

The minimum force sensitivity of an AFM system, limited by Brownian motion [21, 22], can be calculated from $F_{\min} = \sqrt{\frac{4k_B TkB}{\omega_0 Q}}$, where k_B is the Boltzmann constant, T is room temperature, k is the spring constant of the cantilever (3 N/m), B is the bandwidth of measurement (set by lock-in amplifier) used in the force measurement (7.8 Hz), ω_0 is the resonant frequency of the AFM tip (~101 kHz), and Q is the quality factor of the cantilever

(~160) for our measurement parameters. In our setup, this leads to a force sensitivity of ~40 fN. Thus, it should be possible to measure optical force on the order of a fraction of a piconewton with our setup.

The optical force measurement setup uses the modulation of the laser to measure the effect on the amplitude change of the AFM tip at the frequency of modulation of the laser when the AFM tip is brought near the region of optical confinement. The laser is modulated at 50% duty cycle at low frequency (1 kHz) because we have previously shown that phase, and therefore amplitude, require time on the order of ms to respond to an external force [12]. The trigger out of the laser is used as the reference frequency of the lock-in amplifier and the amplitude signal of the AFM is used as the signal in of the lock-in, and the output of the lock-in is fed back to the computer to map to the current position of the AFM tip (see Figure 4).

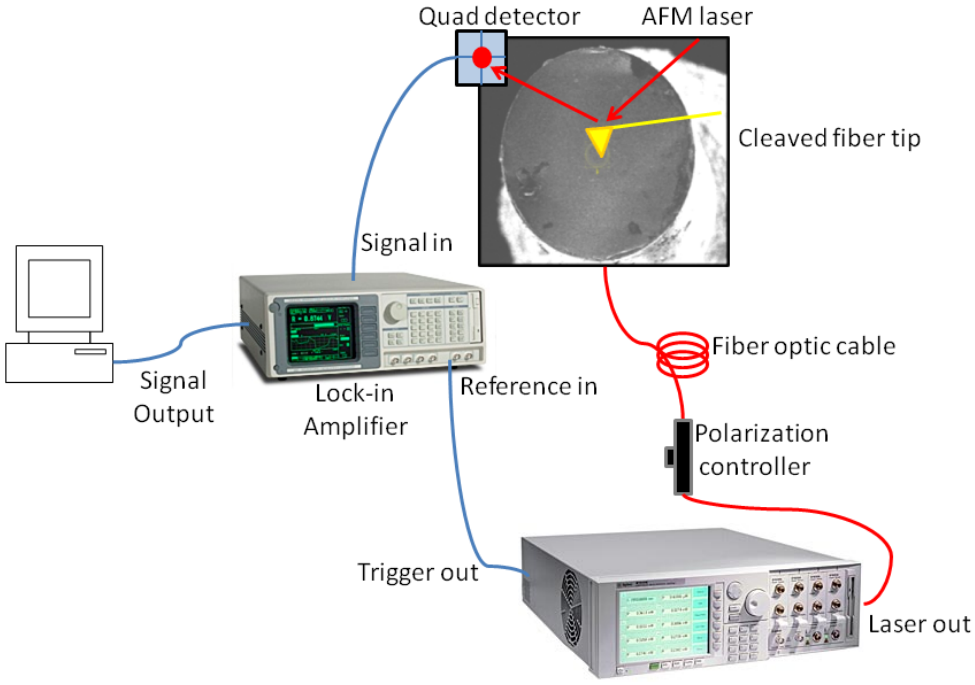

Figure 4 – Setup for measuring optical force.

Figure 5 shows the experimental results of the optical force map. To calculate the optical force from the lock-in output of the above setup we used the following math. First, we took the signal from the lock-in (approx. 0.35 mV) divided by the peak-to-peak signal from the quad detector of the AFM (5 V). This gave us the fractional change in amplitude at 1 kHz of the signal being modulated by the laser, about 7E-5. We then multiplied this by the amplitude of oscillation of the cantilever (30 nm) to get the change in amplitude caused by the laser light (2.1 pm). We then multiplied this by the spring constant of the cantilever (3 N/m) to get the total force (about 6.3 pN). We then subtracted the background noise level when the laser was turned off to get the final value. The experimental result shows a central spot on the order of 0.5 pN and lobes at the end of the bow-tie arms where the force is diminished compared to the central spot, showing good agreement with the simulation. The central spot of the experimental image is likely larger compared to the simulation due to the fact that in the simulation we considered

the AFM tip as a sphere instead of using its actual pyramidal structure. We didn't observe any optical force in the bowtie whose long axis was not aligned with the incident electric field.

The spatial resolution of this technique is limited by two factors, first, the radius of curvature of the AFM tip used for the scan, and second, the bandwidth of the lock-in amplifier used in the experimental setup. For the radius of curvature of the AFM tip, there is a tradeoff – the smaller the radius, the greater resolution, but also smaller interaction with the optical force generated by the nanoantenna, which is why we prefer a tip with a radius of about 100 nm. There is also a tradeoff with bandwidth of the lockin – the greater the bandwidth of the lock-in, the smaller the spot size of the scan will be, but also the noise will be higher. Note that the long term mechanical stability of the sample determines a lower bound on the scan speed, which determines a minimum bandwidth one can choose.

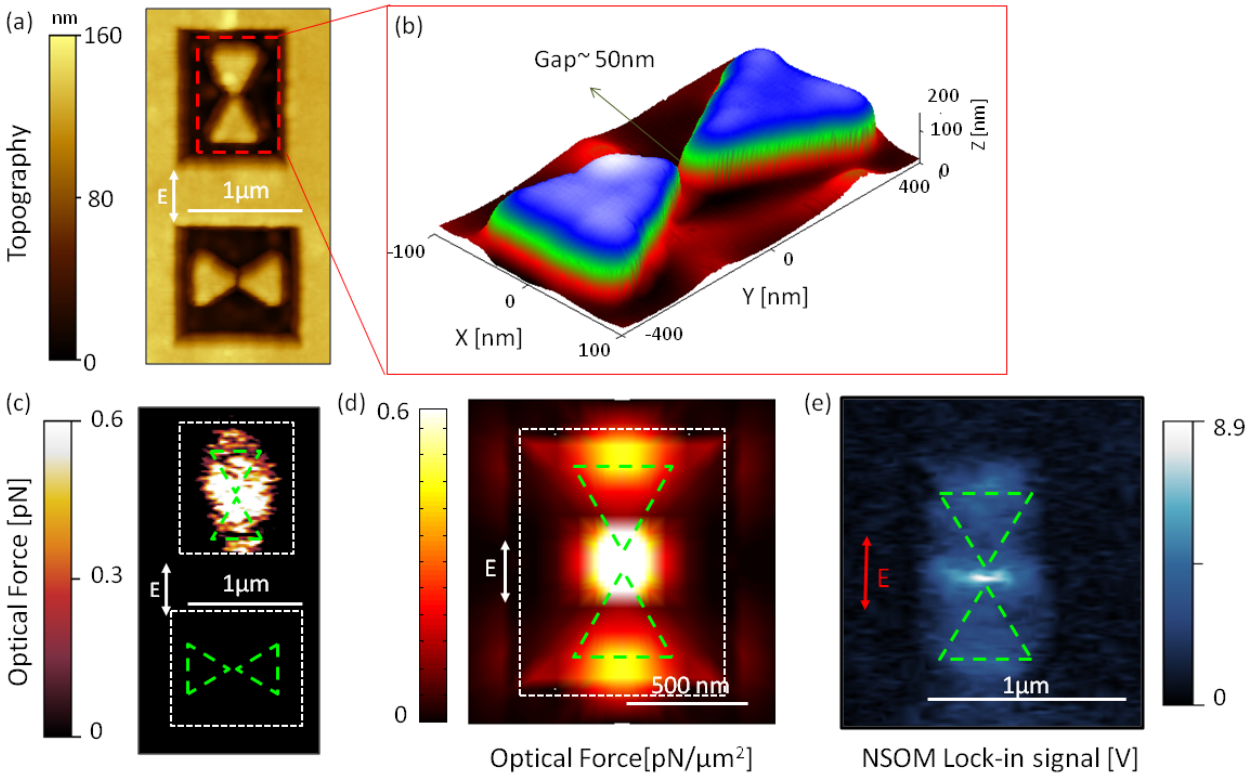

Figure 5 –(a) Topography showing two perpendicularly aligned bowties and (b) 3-D view. The height in the 3-D view is higher than the total design height of 110 nm because of overmilling with FIB. (c) Experimental optical force map. (d) Simulation of optical force map. (e) a-NSOM image showing the near-field map.

5. CONCLUSION

In conclusion, we have presented a method for mapping the optical force intensity created by a plasmonic nanoantenna in non-contact mode with an atomic force microscope. We have used 3-D FDTD simulation to optimize the design of the antenna and simulate the optical force intensity using Maxwell's stress tensor method. The antenna was fabricated on the face of a metal-dielectric-metal coated optical fiber using focused ion beam milling. We have used a home-made aperture less near-field scanning optical microscope to simultaneously measure the topography and near-field intensity of the antenna. Finally, we presented a method to map the optical force generated on the AFM tip due to optical confinement. With dual lock-in amplifiers, this method could map the topography, near-field, and optical force all simultaneously. We believe that this work has many applications in areas ranging from optical trapping in biosensing [23-26] to optical switching in telecommunication [27].

6. REFERENCES

[1] A. Ashkin, J. M. Dziedzic, and T. Yamane, "OPTICAL TRAPPING AND MANIPULATION OF SINGLE CELLS USING INFRARED-LASER BEAMS," *Nature,* vol. 330, pp. 769-771, Dec 1987.

[2] K. T. Gahagan and G. A. Swartzlander, "Optical vortex trapping of particles," *Optics Letters,* vol. 21, pp. 827-829, Jun 1996.

[3] K. C. Neuman and S. M. Block, "Optical trapping," *Review of Scientific Instruments,* vol. 75, pp. 2787-2809, Sep 2004.

[4] H. Xu, auml, and M. ll, "Surface-Plasmon-Enhanced Optical Forces in Silver Nanoaggregates," *Physical Review Letters,* vol. 89, p. 246802, 2002.

[5] A. E. Cetin, A. A. Yanik, C. Yilmaz, S. Somu, A. Busnaina, and H. Altug, "Monopole antenna arrays for optical trapping, spectroscopy, and sensing," *Applied Physics Letters,* vol. 98, Mar 2011.

[6] M. Ploschner, M. Mazilu, T. F. Krauss, and K. Dholakia, "Optical forces near a nanoantenna," *Journal of Nanophotonics,* vol. 4, Feb 2010.

[7] M. Righini, A. S. Zelenina, C. Girard, and R. Quidant, "Parallel and selective trapping in a patterned plasmonic landscape," *Nature Physics,* vol. 3, pp. 477-480, Jul 2007.

[8] M. L. Juan, R. Gordon, Y. J. Pang, F. Eftekhari, and R. Quidant, "Self-induced back-action optical trapping of dielectric nanoparticles," *Nature Physics,* vol. 5, pp. 915-919, Dec 2009.

[9] G. Knoner, A. Ratnapala, T. A. Nieminen, C. J. Vale, N. R. Heckenberg, and H. Rubinsztein-Dunlop, "Optical force field mapping in microdevices," *Lab on a Chip,* vol. 6, pp. 1545-1547, Dec 2006.

[10] G. Volpe, R. Quidant, G. Badenes, and D. Petrov, "Surface plasmon radiation forces," *Physical Review Letters,* vol. 96, Jun 2006.

[11] A. Rodriguez, M. Ibanescu, D. Iannuzzi, J. D. Joannopoulos, and S. G. Johnson, "Virtual photons in imaginary time: Computing exact Casimir forces via standard numerical electromagnetism techniques," *Physical Review A,* vol. 76, Sep 2007.

[12] J. Kohoutek, I. Y. L. Wan, and H. Mohseni, "Dynamic measurement and modeling of the Casimir force at the nanometer scale," *Applied Physics Letters,* vol. 96, Feb 2010.

[13] J. Kohoutek, D. Dey, A. Bonakdar, R. Gelfand, A. Sklar, O. G. Memis, and H. Mohseni, "Opto-Mechanical Force Mapping of Deep Subwavelength Plasmonic Modes," *Nano Letters,* vol. 11, 2011.

[14] H. Raether, *Surface plasmons on smooth and rough surfaces and on gratings*. New York: Springer, 1988.

[15] R. D. Grober, R. J. Schoelkopf, and D. E. Prober, "Optical antenna: Towards a unity efficiency near-field optical probe," *Applied Physics Letters,* vol. 70, pp. 1354-1356, Mar 1997.

[16] D. J. Griffiths, *Introduction to Electrodynamics*, 3 ed. Upper Saddle River, New Jersey: Prentice-Hall, 1999.

[17] D. Dey, J. Kohoutek, R. M. Gelfand, A. Bonakdar, and H. Mohseni, "Quantum-cascade laser integrated with a metal-dielectric-metal-based plasmonic antenna," *Optics Letters,* vol. 35, pp. 2783-2785, Aug 2010.

[18] D. Dey, J. Kohoutek, R. M. Gelfand, A. Bonakdar, and H. Mohseni, "Composite Nano-Antenna Integrated With Quantum Cascade Laser," *Photonics Technology Letters, IEEE,* vol. 22, pp. 1580-1582, 2010.

[19] J. Kohoutek, D. Dey, R. Gelfand, A. Bonakdar, and H. Mohseni, "An apertureless near-field scanning optical microscope for imaging surface plasmons in the mid-wave infrared," in *Novel Optical Systems Design and Optimization Xiii*. vol. 7787, G. G. Gregory and R. J. Koshel, Eds., ed Bellingham: Spie-Int Soc Optical Engineering, 2010.

[20] R. Hillenbrand, B. Knoll, and F. Keilmann, "Pure optical contrast in scattering-type scanning near-field microscopy," *Journal of Microscopy-Oxford,* vol. 202, pp. 77-83, Apr 2001.

[21] J. Kohoutek, I. Y. L. Wan, O. G. Memis, and H. Mohseni, "An opto-electro-mechanical infrared photon detector with high internal gain at room temperature," *Optics Express,* vol. 17, pp. 14458-14465, Aug 2009.

[22] M. Li, H. X. Tang, and M. L. Roukes, "Ultra-sensitive NEMS-based cantilevers for sensing, scanned probe and very high-frequency applications," *Nature Nanotechnology,* vol. 2, pp. 114-120, Feb 2007.

[23] R. M. Gelfand, L. Bruderer, and H. Mohseni, "Nanocavity plasmonic device for ultrabroadband single molecule sensing," *Optics Letters,* vol. 34, pp. 1087-1089, Apr 2009.

[24] L. Huang, S. J. Maerkl, and O. J. F. Martin, "Integration of plasmonic trapping in a microfluidic environment," *Optics Express,* vol. 17, pp. 6018-6024, Apr 2009.

[25] M. Righini, P. Ghenuche, S. Cherukulappurath, V. Myroshnychenko, F. J. G. de Abajo, and R. Quidant, "Nano-optical Trapping of Rayleigh Particles and Escherichia coli Bacteria with Resonant Optical Antennas," *Nano Letters,* vol. 9, pp. 3387-3391, Oct 2009.
[26] R. M. Gelfand, D. Dey, J. Kohoutek, A. Bonakdar, S. C. Hur, D. D. Carlo, and H. Mohseni, "Towards an Integrated Chip-Scale Plasmonic Biosensor," *Optics and Photonics News,* vol. 22, pp. 32-37, 2011.
[27] Z. F. Wang, W. Cao, X. C. Shan, J. F. Xu, S. P. Lim, W. Noell, and N. F. de Rooij, "Development of 1x4 MEMS-based optical switch," *Sensors and Actuators a-Physical,* vol. 114, pp. 80-87, Aug 2004.